

## An electron Talbot interferometer

Benjamin J McMorran<sup>1,2</sup> and Alexander D Cronin

Department of Physics, University of Arizona, Tucson, AZ 85721, USA

E-mail: [mcmorran@nist.gov](mailto:mcmorran@nist.gov)

*New Journal of Physics* **11** (2009) 033021 (7pp)

Received 14 January 2009

Published 17 March 2009

Online at <http://www.njp.org/>

doi:10.1088/1367-2630/11/3/033021

**Abstract.** We report the first demonstration of a Talbot interferometer for electrons. The interferometer was used to image the Talbot carpet behind a nanofabricated material grating. The Talbot interferometer design uses two identical gratings, and is particularly sensitive to distortions of the incident wavefronts. To illustrate this we used our interferometer to measure the curvature of concave wavefronts in a weakly focused electron beam. We describe how this wavefront curvature demagnified the Talbot revivals, and we discuss further applications for electron Talbot interferometers.

The Talbot effect [1], in which a wave imprinted with transverse periodicity reconstructs itself at regular intervals, is a diffraction phenomenon that occurs in many physical systems. Here we present the first observation of the Talbot effect for electron de Broglie waves behind a nanofabricated transmission grating. This was thought to be difficult because of Coulomb interactions between electrons and nanostructure gratings, yet we were able to map out the entire near-field interference pattern, the ‘Talbot carpet’, behind a grating. We did this using a Talbot interferometer, in which Talbot interference fringes from one grating are moiré-filtered by a second grating. This arrangement has served for optical [2], x-ray [3], and atom interferometry [4], but never before for electrons.

In transmission electron microscopy, Talbot revivals (Fourier self-images) behind crystals have been imaged directly, and understanding these revivals is necessary for the correct interpretation of crystal structure [5]. However, direct images of Talbot revivals are not nearly as sensitive to wavefront distortions as the signal from a Talbot interferometer. As we discuss, our arrangement of two nanogratings can easily detect a beam convergence of  $10^{-4}$  radians. Nanogratings have been used recently to construct other types of electron interferometers—a Lau type [6] and a Mach–Zehnder type [7]—but both of these designs are insensitive to wavefront deformations in the incident electron beam.

<sup>1</sup> Author to whom any correspondence should be addressed.

<sup>2</sup> Present address: Electron Physics Group, Center for Nanoscale Science and Technology, National Institute of Standards and Technology, Gaithersburg, MD 20899-8412, USA.

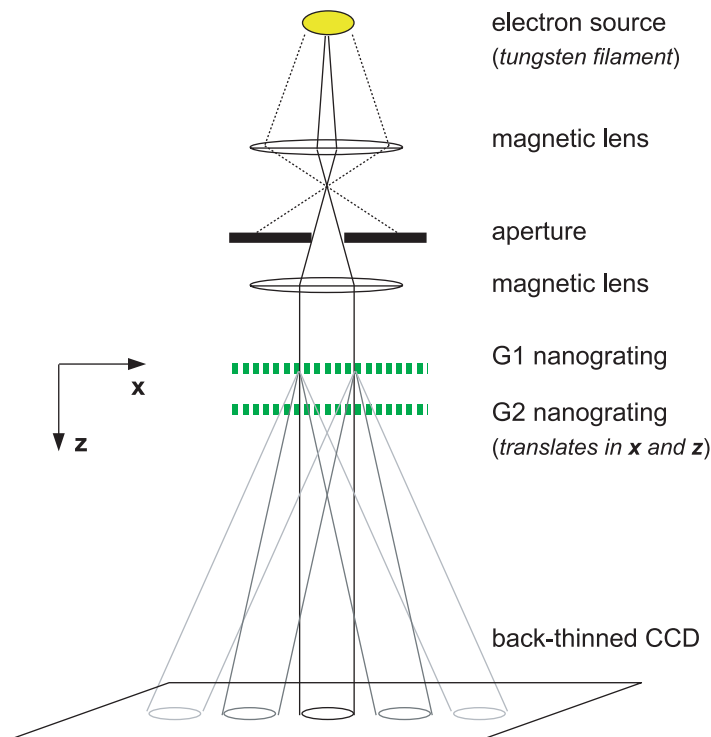


**Figure 1.** Experimental setup. A beam of electrons illuminates a nanoscale transmission grating G1 (at location  $z = 0$  along the optical axis). The resulting near-field interference pattern is read out using a second identical grating G2 (at  $z = 0.1\text{--}1.7$  mm). An imaging detector (at  $z = 1$  m) records the transmitted far-field intensity distribution.

Observations of the Talbot effect with atoms [4, 8] launched many applications for near-field atom optics, such as compound beam splitters for atomic de Broglie waves [9, 10], Talbot–Lau interferometers for atoms and large molecules [11, 12], interferometry with the Poisson spot for atom waves [13], and ‘direct deposit’ lithography of atoms behind phase and absorption gratings [14, 15]. Talbot interferometers have found numerous applications in light optics too, such as imaging phase objects [16], measuring beam collimation [17], and characterizing lenses [18]. For a review see [2]. Recently, nanostructures have been used to build x-ray Talbot interferometers [3, 19], which provide images of phase objects with less x-ray dose delivered to the subject. Imaging phase objects is possible because the Talbot interferometer is a type of shearing interferometer [20, 21], in which a beam is split into multiple overlapping paths. These applications, which have been realized with atoms or photons, suggest potential uses for *electron* Talbot interferometers.

A diagram of our Talbot interferometer is shown in figure 1. Electrons emitted from a heated tungsten filament are accelerated and collimated by a scanning electron microscope optics column [27], resulting in a  $250\ \mu\text{m}$ -diameter beam with an initial current density of approximately  $1\ \mu\text{A cm}^{-2}$ . The beam passes through two consecutive nanofabricated gratings, each consisting of an array of slits etched all the way through a  $150\ \text{nm}$ -thick suspended membrane of low stress  $\text{Si}_3\text{N}_5$  [26]. The gratings have a period  $d = 100\ \text{nm}$  and when coated with a thin metal layer they serve as Ronchi rulings for low energy ( $<10\ \text{keV}$ ) electrons [22].

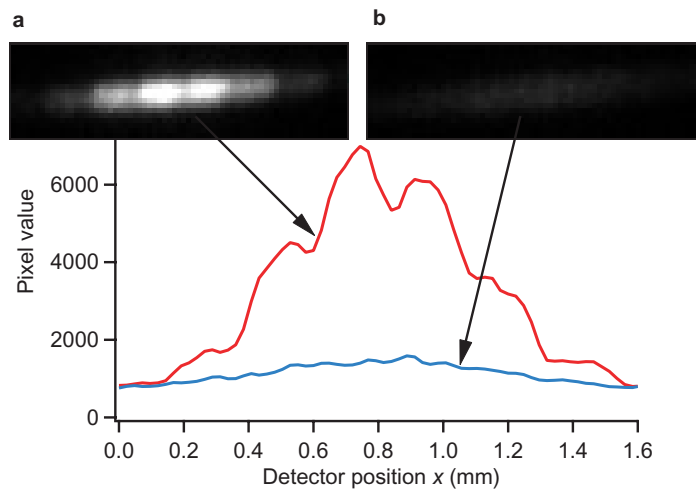


**Figure 2.** Far-field diffraction of electrons transmitted through two nanogratings using a 2.8 keV collimated beam. The gratings were separated by one Talbot distance  $L_T = 0.86$  mm. In (a) the slits of G2 are in registry with the Talbot fringes of G1, and in (b) G2 is shifted in the  $x$ -direction by 50 nm, half a grating period. Line profiles of each image are indicated below them. The asymmetry of diffraction orders (barely resolved due to the wide, collimated beam) is discussed in the text.

A detector located 1 m downstream from the gratings collects images of the transmitted electrons. This detector is a Princeton Instruments PIXIS-XO camera designed for x-ray and EUV imaging, but was used here to directly image low-energy (0.3–5 keV) electrons with high sensitivity. Custom detectors featuring back-thinned CCDs have been used before to directly detect low energy electrons before [28], but to our knowledge this work is the first time a commercially available camera has been demonstrated for this application.

When grating G1 is illuminated by collimated plane waves with wavelength  $\lambda$ , Fourier images (Talbot revivals) of the grating occur at half-integer multiples of the Talbot distance  $L_T = 2d^2/\lambda$ . For 2.8 keV electrons,  $\lambda = 23$  pm and  $L_T = 0.86$  mm. The spatial modulations of these revivals, 100 nm in this case, are too small to resolve with our imaging detector, but they can be analyzed using a second grating G2.

The total flux of collimated electrons transmitted to the far-field is maximum when the slits of G2 line up with the fringes of a Talbot revival from G1, as shown in figure 2(a). In figure 2(b), the transmitted flux is reduced by 77% when G2 is shifted laterally by half a period, since the Talbot fringes are then blocked by G2's grating bars. This modulation of the total transmitted intensity (shown in figure 2) occurs only when the gratings are illuminated by the plane waves of a well-collimated beam.

Images of the entire electron near-field interference pattern behind nanograting G1, also known as Talbot carpets, are shown in figure 3. These data were obtained by scanning the position of analyzing grating G2 throughout the near-field region of G1, in both the  $x$ - and  $z$ -directions, while recording the total transmitted electron intensity. The lateral shift of one grating with respect to the other was accomplished by tilting the pair of gratings about an axis nearly aligned with a grating bar of G1. This explains the limited range of transverse motion when the G1–G2 separation was small.

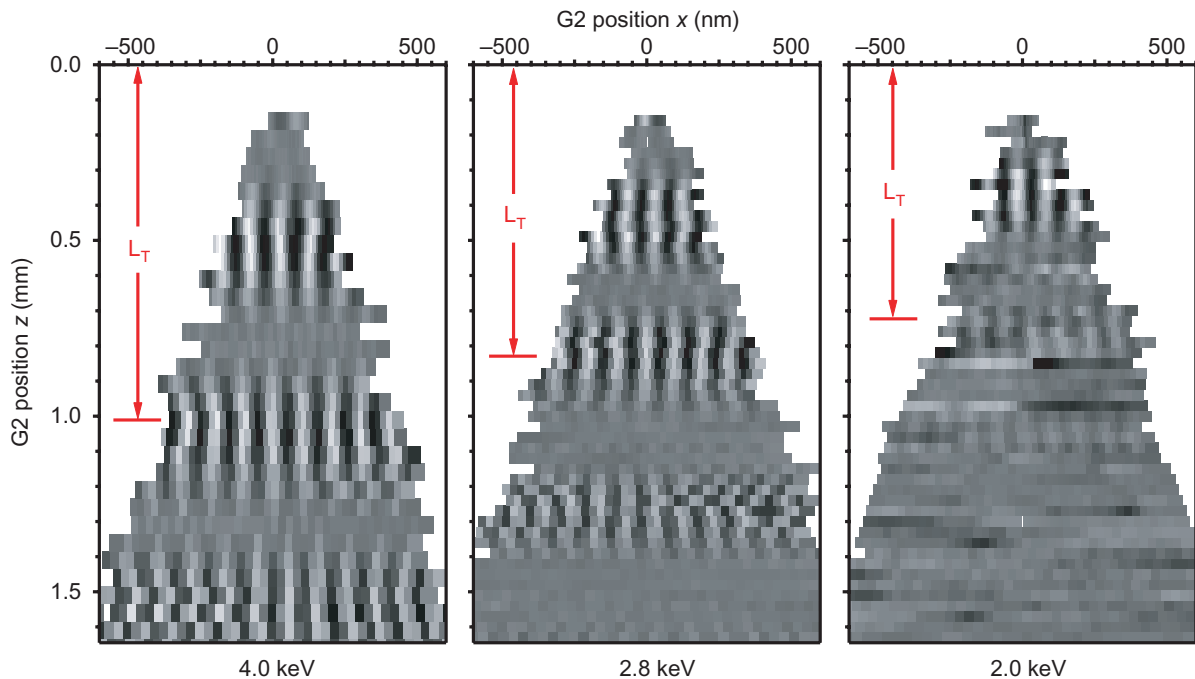


**Figure 3.** Electron near-field interference, or ‘Talbot carpets’, behind a nanograting, using electrons with energy 4 keV (left), 2.8 keV (center), and 2.0 keV (right). The Talbot distance is indicated for each energy (de Broglie wavelength). The value of each pixel is proportional to the total integrated intensity in the far-field diffraction pattern, detected for a particular position of G2 relative to G1. Distortions in these images are due to experimental uncertainty in the position of G2, and are not attributable to distortions in the incident electron waves. The triangular shape of each image is due to the limited lateral scan range at small G1–G2 separations.

When G1 is illuminated with a converging beam, a different type of modulation is observed (figure 4). In this condition, the Talbot revivals from G1 have a finer spatial period than the reference grating G2, due to geometrical demagnification by converging spherical wavefronts. As illustrated in a simulation shown in figure 5, G2 blocks some parts of the beam but not others; i.e. there is a moiré effect between G2 and the interference pattern from G1. This causes dark spots to appear within the resolved far-field diffraction orders. When G2 is scanned laterally, these dark nulls move sideways through the diffraction pattern, as shown in figure 4. This behavior is well described by a general theoretical model of grating interferometers that we developed in [23]. This theory assumes illumination of an arbitrary grating interferometer by a Gaussian Schell-model beam in order to efficiently model the effects of spatial coherence and beam convergence/divergence. The only free parameter in the simulation in the right column of figure 4 was the radius of wavefront curvature of the incident beam. The theory matches the data best by assuming an incident radius of wavefront curvature equal to  $2.15 \pm 0.1$  m—a nearly collimated beam with a convergence angle of  $\sim 75$   $\mu$ rad. Negative diffraction orders in figure 4 have a higher intensity than their positive counterparts, and this asymmetry is understood to result from image–charge (Coulomb) interactions between the grating and transmitted electrons [22].

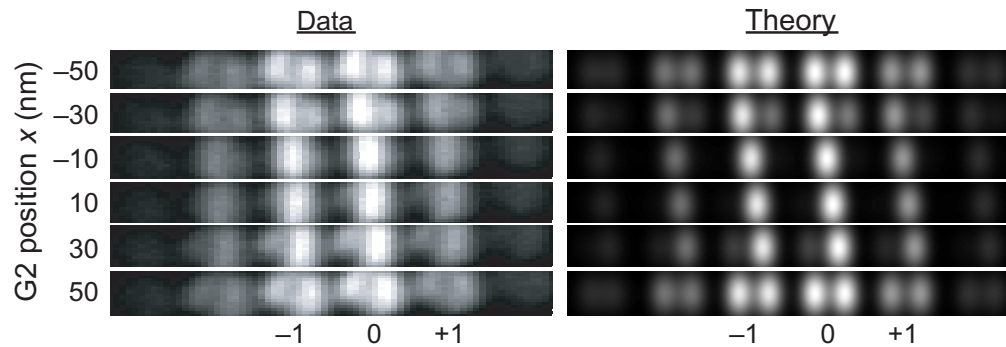


**Figure 4.** The demagnified Talbot effect, indicated by far-field diffraction patterns collected at different lateral positions of G2. The left column is a series of diffraction patterns, with the diffraction orders indicated below them, recorded when using a weakly focused beam of 2 keV electrons. An intensity null moves sideways through each diffraction order as G2 is moved laterally. The simulations in the right column reproduce this modulation, using a model [23] in which G2 filters the demagnified Talbot revival from G1.

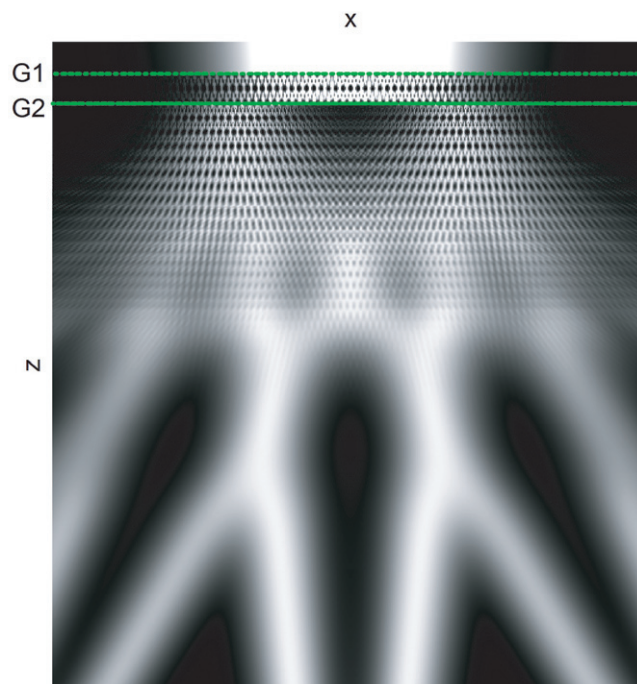


**Figure 5.** Simulation of a Talbot interferometer with a converging incident beam. The Talbot revival has a smaller period than the reference grating. Only the edges of the converging beam are transmitted, which results in two tilted far-field diffraction patterns. This simulation was made using the model developed in [23].

This work shows that the Talbot effect is a way to reproduce periodic structures using electron beams. Similar gratings have been used as masks for projection electron lithography [24]. However, deliberate use of the Talbot effect for lithography would be advantageous because the mask could be located millimeters from the substrate, since a Talbot revival, not a direct shadow, would be used for the exposure. Furthermore, as we have shown here, demagnified Fourier images created using a focused electron beam could be used to construct structures with finer periods than the original (a similar technique has already been demonstrated using UV lithography [25]).

To summarize, we have built a Talbot interferometer for 2.8 keV electrons using two nanofabricated gratings. We used this device to map the near-field interference pattern, known as the Talbot carpet, behind a single grating. Analogous to x-ray and optical Talbot interferometers, this arrangement is very sensitive to deformations in the wavefronts of incoming electrons. We demonstrated this by measuring the 2.1 m radius of wavefront curvature of a focused electron beam, and creating demagnified Talbot revivals with features smaller than the original grating. These results point to future investigations of the imaging and lithographic capabilities of the electron Talbot interferometer.

## Acknowledgments

We acknowledge Manjul Shah at Princeton Instruments for the loan of the PIXIS imaging detector, Tim Savas at MIT for fabricating the gratings, and Mark Robertson-Tessi and Grady Weyenberg for helping to construct the electron beam apparatus. This work was supported by the National Science Foundation grant number PHY-0653623, and by the University of Arizona.

## References

- [1] Talbot H F 1836 Facts relating to optical science *Phil. Mag.* **9** 401
- [2] Paturski K 1989 *Prog. Opt.* **27** 3–108
- [3] Momose A, Kawamoto S, Koyama I, Hamaishi Y, Takai K and Suzuki Y 2003 *Japan. J. Appl. Phys.* **42** L866
- [4] Chapman M S, Ekstrom C R, Hammond T D, Schmiedmayer J, Tannian B E, Wehinger S and Pritchard D E 1995 *Phys. Rev. A* **51** R14
- [5] Spence J C H 2003 *High-Resolution Electron Microscopy* (New York: Oxford University Press)
- [6] Cronin A D and McMorrin B 2006 *Phys. Rev. A* **74** 061602
- [7] Groninger G, Barwick B and Batelaan H 2006 *New J. Phys.* **8** 224
- [8] Nowak S, Kurtsiefer C, Pfau T and David C 1997 *Opt. Lett.* **22** 1430
- [9] Wang Y J, Anderson D Z, Bright V M, Cornell E A, Diot Q, Kishimoto T, Prentiss M, Saravanan R A, Segal S R and Wu S J 2005 *Phys. Rev. Lett.* **94** 090405
- [10] Garcia O, Deissler B, Hughes K J, Reeves J M and Sackett C A 2006 *Phys. Rev. A* **74** 031601
- [11] Clauser J F and Li S F 1994 *Phys. Rev. A* **49** R2213
- [12] Brezger B, Hackermuller L, Uttenthaler S, Petschinka J, Arndt M and Zeilinger A 2002 *Phys. Rev. Lett.* **88** 100404
- [13] Nowak S, Stuhler N, Pfau T and Mlynek J 1998 *Phys. Rev. Lett.* **81** 5792
- [14] Timp G, Behringer R E, Tennant D M, Cunningham J E, Prentiss M and Berggren K K 1992 *Phys. Rev. Lett.* **69** 1636
- [15] McClelland J J, Scholten R E, Palm E C and Celotta R J 1993 *Science* **262** 877
- [16] Lohmann A W and Silva D E 1971 *Opt. Commun.* **2** 413
- [17] Silva D E 1971 *Appl. Opt.* **10** 1980

- [18] Bhattacharya J C and Aggarwal A K 1991 *Appl. Opt.* **30** 4479
- [19] Weitkamp T, Diaz A, David C, Pfeiffer F, Stampanoni M, Cloetens P and Ziegler E 2005 *Opt. Express* **13** 6296
- [20] Bates W J 1947 *Proc. Phys. Soc.* **59** 940
- [21] Ronchi V 1964 *Appl. Opt.* **3** 437
- [22] McMorran B, Perreault J D, Savas T A and Cronin A D 2006 *Ultramicroscopy* **106** 356
- [23] McMorran B and Cronin A D 2008 *Phys. Rev. A* **78** 013601
- [24] Yoshizawa M and Savas T A 2002 *Japan. J. Appl. Phys.* **41** L87
- [25] Yeh W H, Mansuripur M, Fallahi M and Penner R S 1999 *Opt. Commun.* **170** 207
- [26] Savas T A, Schattenburg M L, Carter J M and Smith H I 1996 *J. Vac. Sci. Technol. B* **14** 4167
- [27] Goldstein J I, Newbury D E, Joy D C, Lyman C E, Echlin P, Lifshin E, Sawyer L and Michael J R 2003 *Scanning Electron Microscopy and X-Ray Microanalysis* (New York: Springer)
- [28] Horacek M 2003 *Rev. Sci. Instrum.* **74** 3379